Unified Theory of Oscillator Phase Noise II: Flicker Noise

William Loh, *Student Member, IEEE*, Siva Yegnanarayanan, *Member, IEEE*, Rajeev J. Ram, *Senior Member, IEEE*, and Paul W. Juodawlkis, *Senior Member, IEEE*

***Abstract*—We present a general theory of oscillator phase-noise for perturbations resulting from both white and flicker noise. Although fundamentally different, both noise sources share in common an underlying principle of analyzing noise in the basis of the oscillator. These similarities allow for an integrated description of noise using a common set of equations. With knowledge of the oscillation power, roundtrip delay, and spectrum of injected noise, the phase noise of an oscillator can be determined to high accuracy. We compare our theory to phase-noise measurements of several RF oscillators with these three parameters independently varied. In addition, we also test the validity of our theory against a hybrid optoelectronic oscillator operating under entirely different principles. Excellent agreement is found in all cases.**

***Index Terms*—Colored noise, microwave photonics (MWPs), oscillators, phase noise, RF.**

I. Introduction

NOISE is a problem common to all oscillator systems. Its effect on oscillators can be decomposed into perturbations of amplitude and phase, both of which act to degrade the spectral purity of the generated signal. In typical oscillators, the influence of phase noise is much larger than that of amplitude noise due to various amplitude-limiting mechanisms. These mechanisms include not only the oscillator's intrinsic negative feedback, which maintains loop gain equal to loop loss, but also the saturation of intracavity components (e.g., the amplifier). A complete understanding of oscillator phase noise is therefore essential for realizing future low-noise oscillator systems.

Recently, for the case of white noise, we showed that a common link existed between all oscillators based on the partitioning of noise among the modes of the oscillator [1]. In an open system, the noise appears white over a broad range of frequencies. However, within the confines of a resonant cavity, the noise is forced to couple only into the basis of the system [2], [3]. For white noise, the coupling of noise is equal into the local density of oscillator modes. With increasing intracavity delay, the number of modes increases but is counteracted by a decrease in power coupled into each mode. Note that we use the term 'cavity' throughout this manuscript to denote any general resonant configuration of the oscillator. For the oscillators that we will be analyzing later, the cavity geometry consists of a ring.

Here, we extend our analysis of oscillator phase-noise to the case of low-frequency flicker noise. The case of flicker noise is particularly important as it is what ultimately limits the phase noise of high-performance oscillators, especially at low offset frequencies. In general, the problem of flicker noise is difficult to analyze as both its origin and spectral properties are not well defined. However, as we will show, its interpretation in oscillators becomes greatly simplified if one views the frequency upconversion of noise from the perspective of a gain perturbation.

Historically, both linear time-invariant (LTI) and linear time-varying (LTV) models have been proposed to explain the phenomenon of oscillator phase-noise. Some of the deficiencies of these models have been previously described in [1] and thus will not be repeated here. Instead, our attention will be focused on theories which that treat the effects of flicker noise on oscillators through integration over the frequency noise spectrum associated with the noise process [4]–[7]. This integral becomes unbounded unless restrictions of finite measurement time are taken into account [4], [5], [7], [8]. Here, we will take a similar approach paying careful attention to the effects of measurement. However, in contrast to previous theories, our formulation uses the noise coupled into the oscillating mode to uniquely specify the frequency noise spectrum corresponding to the noise perturbation. Knowledge of this noise is necessary as without it, only the shape of the oscillator's phase-noise spectrum can be determined and not its absolute magnitude.

The goal of this work is to provide a unified description of phase noise applicable to oscillators of both electrical and optical variety. Towards that end, we will show that only three fundamental parameters are necessary to specify the behavior of an oscillator: the spectrum of injected noise, the roundtrip time delay, and the oscillating power. We supplement our theory with measurements of phase noise in RF ring-cavity oscillators and show excellent agreement across multiple configurations and a wide range of operating conditions. Finally, we conclude with comparisons to the phase noise of a hybrid optoelectronic oscillator [9]–[12] to demonstrate the generality of the theory. As was the case in [1], our theory is applicable to any oscillator that can be represented through a gain element and delay wrapped in a positive feedback circuit. Note that the delay does not have to be purely a physical delay but can also include the group delay

Manuscript received May 28, 2013; revised October 17, 2013; accepted October 21, 2013. Date of publication November 13, 2013; date of current version December 02, 2013. This work was supported in part by the Assistant Secretary of Defense for Research and Engineering under Air Force contract #FA8721-05-C-0002.

W. Loh is with the Massachusetts Institute of Technology, Cambridge, MA 02139 USA and with MIT Lincoln Laboratory, Lexington, MA 02420 USA (e-mail: willoh@mit.edu).

S. Yegnanarayanan and P. W. Juodawlkis are with the MIT Lincoln Laboratory, Lexington, MA 02420 USA (e-mail: siva.yegnanarayanan@ll.mit.edu; juodawlkis@ll.mit.edu).

R. J. Ram is with the Electrical Engineering Department, Massachusetts Institute of Technology, Cambridge, MA 02139 USA (e-mail: rajeev@mit.edu).

Color versions of one or more of the figures in this paper are available online at http://ieeexplore.ieee.org.

Digital Object Identifier 10.1109/TMTT.2013.2288205

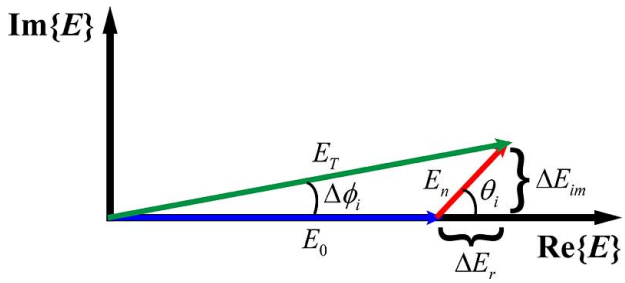

Fig. 1. Vector-based diagram of oscillator field under noise perturbation.

accumulated from signal propagation through a filter resonance. This encompasses a broad range of oscillators operating in both the electrical and optical domains. We will show that these oscillators are all united by a common technique of analyzing noise in the oscillator's basis. The concept of a basis is fundamental to every physical system and thus explains the widespread applicability of our phase-noise model.

II. Phase Noise Theory

A. Description of an Oscillator Under Noise Perturbation

In this section, we formulate a description of oscillator phase noise by working with spectral densities of noise processes in the frequency domain [3]. The frequency domain allows us to avoid ambiguities associated with the time representation of $1/f$ noise. Similar to [2], [3], our theory begins with a phasor description of the oscillator field under noise perturbation (Fig. 1). The initial field magnitude E_0 is normalized such that $E_0^2 = P_0$, where P_0 is the intracavity power of the signal. Without loss of generality, the oscillator's initial phase ϕ is taken to be 0. The addition of a noise event, having magnitude E_n such that $E_n^2 = P_n$ and relative phase θ_i, results in perturbation of both the amplitude and phase of the original oscillating field. If the phase of the noise event is random relative to that of the field, then θ_i becomes uniformly distributed between 0 and 2π. The amplitude of the total signal vector (E_T) is given by

$$E_T^2 = P_0 + \Delta P_i \tag{1}$$

where ΔP_i is defined as the change in oscillation power induced by a noise event having relative phase θ_i. Alternatively, we can define E_T through the vector sum $E_T e^{j\Delta\phi_i} = E_0 + \Delta E_r + j\Delta E_{im}$. Multiplying by its complex conjugate, we find

$$E_T^2 \approx E_0^2 + 2E_0\Delta E_r \tag{2}$$

where we have assumed $E_0 >> \Delta E_r, \Delta E_{im}$. The change in angle of the oscillating field $(\Delta\phi_i)$ can similarly be found through

$$\Delta\phi_i \approx \frac{\Delta E_{im}}{E_0} \tag{3}$$

where again we have assumed $E_0 >> \Delta E_r, \Delta E_{im}$. Note that these approximations represent the linearization of changes in power and phase due to a *single* noise event [1].

It is clear from (1) and (2) that the fluctuation in power is related to the beating between the signal field and the in-phase component of the noise. We may change to units of fluctuation rates through the identification of $F_P(t)$ with ΔP_i and $F_r(t)$ with ΔE_r. $F_p(t)$ and $F_r(t)$ now represent the contribution rate of noise events to fluctuations of the oscillator power and in-phase field with their time dependencies made explicit. These quantities are equivalent to the force terms that describe noise perturbation in Langevin analysis [13]. The corresponding Langevin equations for $F_p(t)$ and $F_r(t)$ are given as

$$\begin{aligned}\frac{d\Delta P(t)}{dt} &= F_P(t)\\ \frac{d\Delta E_r(t)}{dt} &= F_r(t).\end{aligned} \tag{4}$$

$F_p(t)$ and $F_r(t)$ are related through

$$F_P(t) = 2\sqrt{P_0}F_r(t). \tag{5}$$

Similarly, defining $F_\phi(t)$ and $F_{im}(t)$ as the contribution rate of noise events to fluctuations of the oscillator phase and out-of-phase field, the corresponding Langevin equations are then given by [3]

$$\begin{aligned}\Delta\Omega(t) = \frac{d\Delta\phi(t)}{dt} &= F_\phi(t)\\ \frac{d\Delta E_{im}(t)}{dt} &= F_{im}(t).\end{aligned} \tag{6}$$

Here, $\Delta\Omega(t)$ represents the fluctuations in the instantaneous frequency of the oscillating field. From (3), $F_\phi(t)$ and $F_{im}(t)$ are related through

$$F_\phi(t) = \frac{F_{im}(t)}{\sqrt{P_0}}. \tag{7}$$

Although (4) and (6) are expected to be general across all noise processes, the Langevin analysis is typically only applied for the case of white noise. However, we note that any colored noise distribution can be built up from a collection of statistically-independent Ornstein-Uhlenbeck processes with varying damping rate [8]. If necessary, one can readily construct a system of Langevin equations to model the effects of flicker noise.

We may take the autocorrelation of (5) and (7) obtaining $\langle F_P(t)^* F_P(t+\tau)\rangle$ and $\langle F_\phi(t)^* F_\phi(t+\tau)\rangle$, respectively. Here, τ represents the time delay of the correlation. After Fourier transformation into the frequency domain, the following relations between spectral densities can be defined

$$S_{F_P}(\omega) = 4P_0 S_{F_r}(\omega) \tag{8}$$

$$S_{F_\phi}(\omega) = \frac{S_{F_{im}}(\omega)}{P_0}. \tag{9}$$

$S_{F_\phi}(\omega), S_{F_P}(\omega), S_{F_r}(\omega), S_{F_{im}}(\omega)$ in (8) and (9) represent spectral densities corresponding to fluctuation rates of the oscillator phase, power, in-phase field, and out-of-phase field, respectively.

In order to proceed further, these spectral densities must be completely specified. To do so, we consider a generic representation of an oscillator in the geometry of a ring containing a localized region where amplification occurs. If we take the perspective of a signal travelling along the cavity, we would

see that the signal undergoes amplification and noise injection with every pass through the amplifier. Within the confines of the oscillator boundaries, the noise is forced to emit only into the modes of the oscillator, which together form the oscillator's basis. Previously in our analysis of white noise [1], we showed that each mode received a fraction of the noise power according to the local density of modes. In one dimension and for a single polarization, the density of modes is given by the roundtrip delay of the cavity (T), so that the number of modes within a differential frequency interval Δf is equal to $T\Delta f$. The spectral density of the noise ($N_{psd,tot}(\omega)$) within Δf becomes distributed into these modes such that each mode receives a noise power of $N_{psd,tot}(\omega)/T$. In the limit where the spectral width of the noise only encompasses a few cavity modes, the majority of the noise couples into those modes [14], [15]. Note that this analysis can also be extended to cavities of higher dimensionality and polarization, but care must be taken when accounting for any spectral dependence of the mode density.

Our previous discussion is consistent with quantum mechanical formulations of thermal noise [16], [17] where each mode occupies an average energy $k_B T_0$, and thus the power coupled into each mode is $k_B T_0/T$. Here, T_0 denotes the equilibrium temperature of the system. Since there are $T\Delta f$ modes within a frequency interval Δf, the total noise power delivered by all the modes within Δf is $k_B T_0 \Delta f$, which agrees with conventional expressions for the integrated power spectral density of thermal noise.

We now return to (8) to first determine $S_{F_P}(\omega)$ for the case of white noise, later extending the analysis to colored noise. Examining (8), we see that $S_{F_P}(\omega)$ is inherently related to the beating between the in-phase component of noise ($N^r_{psd,tot}(\omega)/T$) and the signal (P_0). Here, ($N^r_{psd,tot}(\omega)$) is the power spectral density of the in-phase noise (assumed white) added in one roundtrip of the cavity. Dividing this noise by T yields the total in-phase noise partitioned into the oscillating mode over the course of the roundtrip. Note that as mentioned earlier, this analysis implicitly assumes a one-dimensional cavity operating in a single polarization state [1]. $N^r_{psd,tot}(\omega)$ is related to $N_{psd,tot}(\omega)$ by a factor of 2 [3]. This factor assumes that half the total noise contributes to in-phase fluctuations. The equal splitting of noise into amplitude and phase is a consequence of the randomness of noise such that the noise does not preferentially align along any particular field direction (Fig. 1). Combining these statements with (8), one can obtain the following form for $S_{F_P}(\omega)$

$$S_{F_P}(\omega) = \frac{4N^r_{psd,tot}(\omega) P_0}{T^2}. \tag{10}$$

Note that (10) introduces one additional factor of T, which accounts for the injection of one roundtrip's worth of noise at a rate inverse to the roundtrip time. This factor of T is a consequence of defining noise fluctuations in terms of fluctuation rates. Although (10) was not a result of rigorous derivation, its form agrees with an analogous equation for lasers obtained independently through Langevin analysis [3]. Furthermore, we will see that (10) also leads to a final phase-noise spectrum equivalent to that derived in [1].

We wish now to extend (10) so that it may be applied to the case of colored noise. Our approach is to simply allow $N^r_{psd,tot}(\omega)$ to vary according to the shape of the noise process. We will see that this approach yields spectral densities of fluctuating variables that acquire the spectral shape of the noise process itself. However, it should be mentioned that some subtleties arise from our handling of colored noise in this manner. For example, one concern is whether the rest of (10) remains self-consistent within our interpretation of $N^r_{psd,tot}(\omega)$. In particular, we note that one of the factors of T in (10) accounts for the total amount of noise coupled into the oscillating mode per cavity roundtrip. For white noise, $N^r_{psd,tot}(\omega)/T$ is intuitive as it corresponds to the noise power spectral density partitioned into the local density of cavity modes [1]. We have not yet shown why this term remains unmodified for the case of flicker noise especially since its spectrum is no longer white. A secondary concern also exists pertaining to how low-frequency flicker noise couples into the oscillation at optical or RF frequencies. These topics will be delegated to the next section.

To proceed further, we require the use of (8)–(10) for determining $S_{F_\phi}(\omega)$. The first step of this procedure involves dividing (10) by $4P_0$ (as per (8)) to recover

$$S_{F_r}(\omega) = \frac{N^r_{psd,tot}(\omega)}{T^2}. \tag{11}$$

Next, we relate $S_{F_{im}}(\omega)$ to $S_{F_r}(\omega)$. Note that if the noise is completely random, the in-phase and out-of-phase noise contributions are equal. This condition applies to conventional white noise but does not necessarily apply to all noise processes. In order to provide a general relation between $S_{F_{im}}(\omega)$ and $S_{F_r}(\omega)$, we define a factor X such that $S_{F_{im}}(\omega) = X S_{F_r}(\omega)$. X is equal to 1 for white noise but may be a different factor if the total noise power splits unevenly between amplitude and phase. We combine the factor of X with $N^r_{psd,tot}(\omega)$ in (11) to recover $N^{im}_{psd,tot}(\omega)$ in the definition of $S_{F_{im}}(\omega)$. Finally, after dividing by P_0 (as per (9)), we obtain

$$S_{F_\phi}(\omega) = \frac{N^{im}_{psd,tot}(\omega)}{P_0 T^2}. \tag{12}$$

B. Flicker Noise in Oscillators

Equation (12) can be used to determine the spectral density of frequency fluctuations and subsequently to calculate the phase-noise spectrum of the oscillator. However, before doing so, let us first examine the topic of flicker noise and address how it affects the modes of the oscillator. Critical to this discussion is the method by which flicker noise evolves from an inherently near-DC phenomenon into a noise source at RF or optical frequencies.

To begin, consider the scenario where an ideal signal passes through an amplifier so that the output consists of a scaled version of the input signal but degraded by noise. Our focus will be on flicker noise since the system behavior under additive white noise has already been analyzed in our earlier work [1]. Following [18], we see that the flicker noise near the signal frequency results from a frequency upconversion process, as the

noise is not present in the absence of a carrier. However, in contrast to [18], we believe the flicker noise upconversion to be intrinsic to the operation of the gain medium itself. That is, an amplifier functions by converting DC voltage/current into gain at frequencies extending to the bandwidth of the amplifier. Near-DC amplifier noise, generated externally by the voltage/current source or internally by traps/defects [19] within the amplifier, results in perturbation of the amplifier gain and therefore affects all signals being amplified. As the amplification process is multiplicative, the resulting RF flicker noise will be proportional to the output signal level.

This can be more concretely seen from the amplifier input-output relations given as

$$E_{out}(t) = [G + \Delta G(t)] E_{in}(t) \tag{13}$$

where G denotes the amplifier's field gain. $\Delta G(t)$ represents a time-dependent perturbation to the gain, which we attribute to be due to low-frequency flicker noise, and $E_{in}(t)$ ($E_{out}(t)$) represents the amplifier's time-dependent input (output) field. Note that in (13), we have ignored the contribution from white noise, which would introduce an additive noise term to the amplified input. This viewpoint of gain is general to any amplifier system. If a near-DC gain fluctuation ($\Delta G(t)$) is introduced, it is clear that this fluctuation propagates to the amplifier output through multiplication by E_{in}. Thus, even if the magnitude of $\Delta G(t)$ remains constant, the observed output noise will rise or fall with the input signal level. Note that $\Delta G(t)$ may be introduced from flicker-noise fluctuations in the power supply or from defects/traps within the amplifier. As any signal within the bandwidth of the amplifier experiences gain, those signals all feel the effect of the noise perturbation. However, the upconverted noise for each mode ultimately depends on the strength of that particular mode (13). Since the strength of the oscillating mode is much larger than that of the sidemodes, the flicker noise predominantly resides around the oscillating mode.

The preceding discussion describes the process by which flicker noise upconverts into the frequency band of oscillation. In the white noise case, the noise provides a direct kick to the system, and the strength of the kick couples equally into each of the available oscillator modes. In the flicker noise case, the noise provides a perturbation to the gain, which then becomes upconverted and is coupled into the oscillator modes. However, we have not yet shown how to determine the amount of flicker noise coupled into each mode. Quantifying the noise into the oscillating mode is especially difficult due to the $1/f^{\alpha}$ spectral dependence of flicker noise. For example, integration over the $1/f$ spectral density would yield an unbounded amount of added noise power. One can potentially circumvent this issue by defining cutoff frequencies for the noise process. However, after integration, one is then left with cumbersome logarithmic quantities dependent on the chosen integration limits. In the end, the noise coupled into the oscillating mode must reproduce a second factor of $1/T$ to be consistent with (10)–(12). We will show in Section III that this $1/T^2$ dependence is *necessary* to yield agreement with experimental observation.

One possible resolution to this issue can be seen from (11) by equating $S_{F_r}(\omega)$ to the Fourier transform of $\langle F_r(t)^* F_r(t+\tau)\rangle$ where τ is the time delay of the correlation. As noted earlier, one factor of T accounts for the rate at which the integrated roundtrip noise is added into the cavity. We established that (11) is valid for white noise, and it is clear that for this case the correlation $\langle F_r(t)^* F_r(t+\tau)\rangle$ must be proportional to $\delta(\tau)$ to recover the spectral properties of the noise [3]. The remaining terms $(N^r_{psd,tot}/T)$ of the correlation yield the strength of the total in-phase noise partitioned into the available oscillator modes.

Let us now examine the case of flicker noise using the same approach as before but letting $N^r_{psd,tot}(\omega)$ vary over frequency. Here, we assume the flicker noise process to be stationary, modeled from an ensemble of statistically independent random processes [8]. The Fourier transform of the correlation $\langle F_r(t)^* F_r(t+\tau)\rangle$ provides the desired $1/f^{\alpha}$ shape of the flicker noise spectrum. The remaining terms $(N^r_{psd,tot}/T)$ of the correlation again appear to yield a partitioning of noise similar to the case of white noise. This analysis suggests that the underlying processes of flicker noise are also distributed into the local density of cavity modes, whereas the color of the spectrum is introduced from the correlation between noise events.

C. Oscillator Phase-Noise Spectrum

Having established a useful interpretation of flicker noise, we are now ready to continue with our treatment of oscillator phase-noise. Our starting point is the Langevin equation for fluctuations in the instantaneous frequency ($\Delta\Omega(t)$) defined through (6). Note that we have not included any terms governing the coupling of amplitude and phase [2], [3] in (6). Should the need arise, one can readily define an equivalent "linewidth enhancement factor" for any oscillator system. The autocorrelation of (6) can be found through $\langle \Delta\Omega(t)^* \Delta\Omega(t+\tau)\rangle$. Subsequent application of the Fourier transform yields

$$S_{\Delta\Omega}(\omega) = S_{F_\phi}(\omega) = \frac{N^{im}_{psd,tot}(\omega)}{P_0 T^2} \tag{14}$$

where $S_{\Delta\Omega}(\omega)$ is defined as the spectral density of frequency fluctuations. It is clear that $S_{\Delta\Omega}(\omega)$ follows the same spectral dependence as that exhibited by the noise process itself. With $S_{\Delta\Omega}(\omega)$ defined, one can then determine the variance in the oscillator's phase fluctuations $\langle\Delta\phi^2(\tau)\rangle$[3]–[7], [20] from

$$\langle \Delta\phi^2(\tau)\rangle = \frac{2}{\pi}\int_{-\infty}^{\infty} S_{\Delta\Omega}(\omega)\frac{\sin^2\left(\frac{\omega\tau}{2}\right)}{\omega^2} d\omega. \tag{15}$$

Equation (15) provides the result necessary for obtaining the oscillator's phase-noise spectrum. To show this, we apply the Wiener-Khinchin theorem beginning with the autocorrelation function of the electric field. When the oscillator's amplitude noise is negligible compared to its phase noise, this autocorrelation becomes [1]

$$\langle E(t)^* E(t+\tau)\rangle \approx E_0^2 e^{j2\pi f_0\tau} e^{-\langle\Delta\phi^2(\tau)\rangle/2} \tag{16}$$

where f_0 is the frequency of oscillation. Note that (16) assumes that the phase fluctuations are Gaussian distributed (via the Central Limit Theorem) [1]. The Fourier transform of (16) yields the desired phase-noise spectrum of the oscillator centered at

its oscillation frequency. Division by $P_0 = E_0^2$ is also required in order to normalize the spectrum to the carrier power.

We now apply (14)–(16) to the calculation of phase noise for an oscillator perturbed by both white and $1/f$ noise. The sum of both noise contributions can be compactly represented through

$$S_{\Delta\Omega}(\omega) = \frac{1}{P_0 T^2}\left(N_0^{im} + \frac{N_1^{im}}{|\omega|}\right) \tag{17}$$

where N_0^{im} is the strength of the phase component of white noise at any particular frequency and N_0^{im} is the strength of the phase component to $1/f$ noise at 1 rad/s. Note that N_0^{im} differs from the usual $1/f$ flicker-noise coefficient by a factor of 2π since we have represented the noise in angular frequency units. The individual contributions of white and $1/f$ noise are separable and can be independently evaluated in (15). For white noise, we find

$$\left\langle \Delta\phi^2(\tau)\right\rangle_W = \frac{N_0^{im}|\tau|}{P_0 T^2}. \tag{18}$$

With the identification of $N_0^{im} = N_{psd,tot}/2$, (18) is identical to (11) of [1] whose derivation makes use of a vector-based approach to phase noise.

The same process used to determine (18) can in principle be applied to the case of $1/f$ noise. Doing so, one finds that the integral of (15) diverges to infinity when integrating through $\omega = 0$. This divergence is a direct consequence of the large increase in noise power as the frequency approaches the carrier. However, in real (physical) systems, the measurement time is always restricted, and the bandwidth is always finite. These conditions present bounds on both the minimum and maximum frequencies that effectively contribute to the measurement. Some discussion is warranted regarding how these bounds are implemented within the framework of (15).

For this discussion, we consider a thought experiment taking the perspective of the measurement system whose purpose is to determine the phase noise of an oscillator. Our first task is to obtain a finite-length sample of the oscillator field. The field we measure consists of a periodic signal embedded in random fluctuations due to noise. We next take the field's autocorrelation as per (16) so that the spectrum may be computed from its Fourier transform. It is clear that if the noise fluctuations of interest occur slower than the time allotted to our field sampling, then these fluctuations are effectively *invisible* to the measurement. This introduces a low-frequency limit, below which the noise contributions become approximately zero to the integral of (15). Note that the original statement of (15) has the interpretation that all frequencies of $S_{\Delta\Omega}(\omega)$ contribute to the observed phase noise. A similar line of reasoning also follows for the high-frequency limit where it is now the measurement bandwidth that renders higher frequencies of noise to zero. However, since the integrand in (15) consists of decaying functions with frequency, we choose instead to keep $\pm\infty$ as the high-frequency limit with negligible loss to accuracy. This choice simplifies the number of variable definitions necessary to the setup of the integral.

We may now evaluate (15) for $1/f$ noise with the help of a lower frequency cutoff (ω_c). With this bound in place, the previous issues of divergence are circumvented. Note that in defining ω_c, we have introduced an abrupt cutoff in the frequencies that contribute to measurable phase fluctuations. Should the need arise, a more gradual rolloff can readily be used. The integral for $1/f$ noise can be calculated by first recognizing that the integrand is even and subsequently introducing ω_c as the lower frequency limit. This integration yields

$$\left\langle \Delta\phi^2(\tau)\right\rangle_{1/f} = \frac{N_1^{im}\tau^2}{\pi P_0 T^2}\left(\frac{\sin^2\left(\omega_c\frac{\tau}{2}\right)}{2\left(\omega_c\frac{\tau}{2}\right)^2} + \frac{\sin(\omega_c\tau)}{\omega_c\tau} - Ci(\omega_c|\tau|)\right) \tag{19}$$

where $Ci(\omega_c|\tau|)$ represents the cosine integral of its argument. To maintain self-consistency with our chosen cutoff frequency, τ must be restricted so that $\omega_c|\tau| < 2\pi$. This condition expresses the fact that although we have accounted for ω_c introduced by the finite length of our sampled field, we have not limited the time delay of our autocorrelation function ((16)). Clearly, $|\tau|$ must be less than the duration of the field $(2\pi/\omega_c)$ for the overlap of the fields to be meaningful. Having established $\omega_c|\tau| < 2\pi$, we ideally would like to proceed further and simplify (19) using $\omega_c|\tau| << 1$. However, as it stands, it appears that some error would be incurred in making this approximation when $\omega_c|\tau|$ is close to 2π. In actuality, this error is negligible for a wide variety of cases. Substitution of (19) into (16) shows that the exponential of the autocorrelation becomes a strong function of τ. We are specifically interested in showing this exponential to be negligible in the range of large τ. This becomes true for typical values of $\omega_c \sim 1$ rad/s and under typical levels of $1/f$ noise injection. For these cases, we may approximate (19) using $\omega_c|\tau| << 1$ to obtain

$$\left\langle \Delta\phi^2(\tau)\right\rangle_{1/f} = \frac{N_1^{im}\tau^2}{\pi P_0 T^2}\left(\frac{3}{2} - \gamma - \ln(\omega_c|\tau|)\right) \tag{20}$$

where $\gamma \approx 0.5772$ is the Euler-Mascheroni constant. In Section III, we will show examples where we justify this approximation for use in calculating the phase noise of an oscillator. Furthermore, we will also apply (14)–(16) to noise exhibiting $1/f^\alpha$ dependence with values of α other than 0 or 1. Note that approximating $\omega_c|\tau| << 1$ introduces a sign reversal from positive to negative in (20) when $\omega_c|\tau| \sim 2.5$. Beyond these limits $\left\langle \Delta\phi^2(\tau)\right\rangle_{1/f}$ must be set to infinity in order to prevent this artifact from distorting the computations of (16).

To evaluate the total phase-noise spectrum, we combine (18) and (20) in (16) and take the Fourier transform of the result. We also normalize to the carrier power through division by P_0. The combined spectrum consists of the convolution between the individual phase-noise contributions due to white and $1/f$ noise. The white-noise contribution leads to a Lorentzian, while the spectrum due to $1/f$ noise must be evaluated numerically. It is clear from (18)–(20) that the phase variance is dependent on the ratio of noise to signal and on the square of the roundtrip delay. To reduce phase noise, the noise should be minimized relative to the oscillating signal. This can be easily achieved for white noise through an increase in intracavity power. However, this method becomes ineffective for the case of flicker noise whose noise is approximately proportional to signal power. Note that in (19) and (20), the noise and signal terms are not independent.

For these cases, the roundtrip delay must be increased in order to gain significant reductions in phase noise.

D. Modeling Procedure: Oscillator Phase-Noise

In this section, we provide a step-by-step prescription detailing how to apply our developed theory to the modeling of oscillator phase-noise. The overarching goal is to determine the oscillator's phase-noise spectrum from the Fourier transform of (16). Note that normalization by $P_0 = E_0^2$ is also required to maintain consistency with traditional definitions of phase noise. Equation (16) depends critically on $\langle \Delta\phi^2(\tau) \rangle$, which can be derived from (14) and (15) once the appropriate variables (i.e., the noise-to-signal ratio and the roundtrip delay) are specified. $\langle \Delta\phi^2(\tau) \rangle$ can also be directly calculated from (18) for the case of white noise and from (19) and (20) for $1/f$ noise. Below, we summarize the steps required for the modeling of oscillator phase-noise.

First, the total phase-noise spectrum injected into the oscillator in one roundtrip of the cavity is measured. This noise can be due to the amplifier alone or to multiple components within the oscillator cavity. In the next section, we will quantify this noise from measurements of the residual noise added in a single roundtrip. This process also allows the determination of the corresponding signal power under oscillation. Note that the individual components of the cavity should be operated (i.e., current and voltage) and also driven (i.e., the signal input) under their appropriate oscillating conditions. The ratio of the noise spectrum to the signal power specifies half of the unknown variables in (14).

Second, the time delay of the system in the vicinity of the oscillating mode is measured. This specifies the rest of the unknown parameters in (14). The roundtrip delay can be found from the frequency translation of the mode corresponding to a 2π shift in phase. An alternative method is to directly probe the S21 response of the system and to subsequently determine the group delay from the slope of the unwrapped phase. For the measurements that we will be conducting in the next section, we measure the roundtrip delay from the frequency separation between cavity sidemodes.

Third, once (14) is specified, the calculation of (15) is applied to determine $\langle \Delta\phi^2(\tau) \rangle$ subject to the appropriate cutoff frequency. Using $\langle \Delta\phi^2(\tau) \rangle$ in (16), normalizing the result by P_0, and subsequently numerically evaluating the Fourier transform yields the desired oscillator phase-noise spectrum.

III. Experimental Results

A. Comparisons to Measurement: Electrical Oscillator

In this section, we will compare the phase-noise theory of (14)–(16) to phase-noise measurements of three different RF ring-cavity oscillators operating at 2.5 GHz. These oscillators all share the same generic ring architecture of Fig. 2 but differ in the type of RF amplifier used. RF isolators were employed at the input and output of each amplifier to allow only for unidirectional oscillation. The output of the amplifier was then sent to an output coupler where the majority (90%) of the RF power was coupled out of the cavity. The remainder (10%) of the power was recirculated within the cavity to drive self-oscillation. The other intracavity elements of the oscillator include an RF filter for defining the oscillator operating frequency, an RF phase shifter for tuning the oscillation frequency, and a variable RF attenuator for controlling the operating point of the oscillator. We wish to emphasize that the signal is coupled out directly after the amplifier prior to any RF filtering (Fig. 2). This allows us to directly measure the noise power added by the amplifier in each roundtrip of the cavity before this noise is rejected by the filter [1]. Note that there is no accumulation of noise power at frequencies outside of the filter passband as the noise is rejected before the completion of each cavity roundtrip.

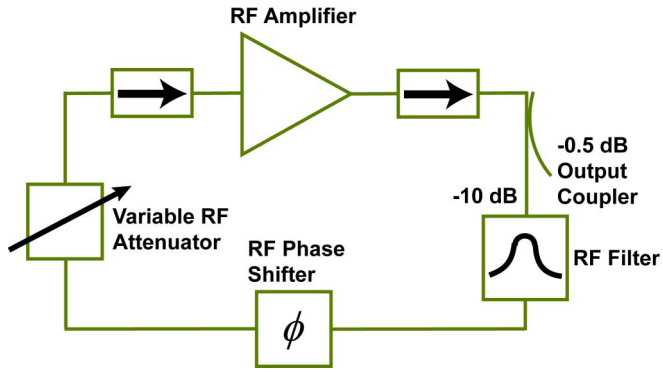

Fig. 2. Generic system diagram employed for three RF oscillators comprising different types of RF amplifiers. The system delay is defined by various configurations of RF filters controlling the net group delay per cavity roundtrip. The RF signal is coupled out prior to filtering allowing for direct measurement of the noise added in each roundtrip.

1) Phase-Noise Measurement: For each RF amplifier used, we measured the oscillator phase-noise under three different configurations of the RF filter. These configurations consist of: (i) a tunable RF filter (halfwidth $(HW) = 75$ MHz at 2.5 GHz), (ii) a tunable RF filter $(HW = 75$ MHz) with 5.5 m additional delay, and (iii) a fixed RF filter $(HW = 2.9$ MHz). For each configuration, the center frequency was 2.5 GHz. By altering the RF filter configuration, we are able to adjust the group delay (and thus roundtrip time) induced by the resonance of the filter.

The results of the phase-noise measured by an Agilent E5052B signal-source analyzer (SSA) are shown in Fig. 3. Note that the measurements for each amplifier were performed at two separate operating conditions controlled by the bias voltage of the amplifier. At each operating point, the amplifier voltage, intracavity loss, and output power were maintained constant over all three filter configurations tested. The primary effect of the different filter configurations is then to vary the roundtrip delay experienced by the oscillating mode of the cavity. The three amplifiers used for our measurements are as follows: Amplifier 1 – Advantek AM-4080 M 2–4 GHz (Figs. 3(a) and 3(b)), Amplifier 2 – Miteq AFS4–02000800-45–10P 2–8 GHz (Figs. 3(c) and 3(d)), and Amplifier 3 – Miteq AM-3A-0520–0 0.5–2 GHz (Figs. 3(e) and 3(f)). Amplifier 3 continues to provide gain at 2.5 GHz (although significantly reduced) despite its maximum specified operating frequency of 2 GHz. We choose this amplifier to demonstrate the wide range of cases that our theory is applicable to. We will first, however, describe our measured phase-noise results for these three amplifiers and neglect for the moment the phase noise predicted by theory.

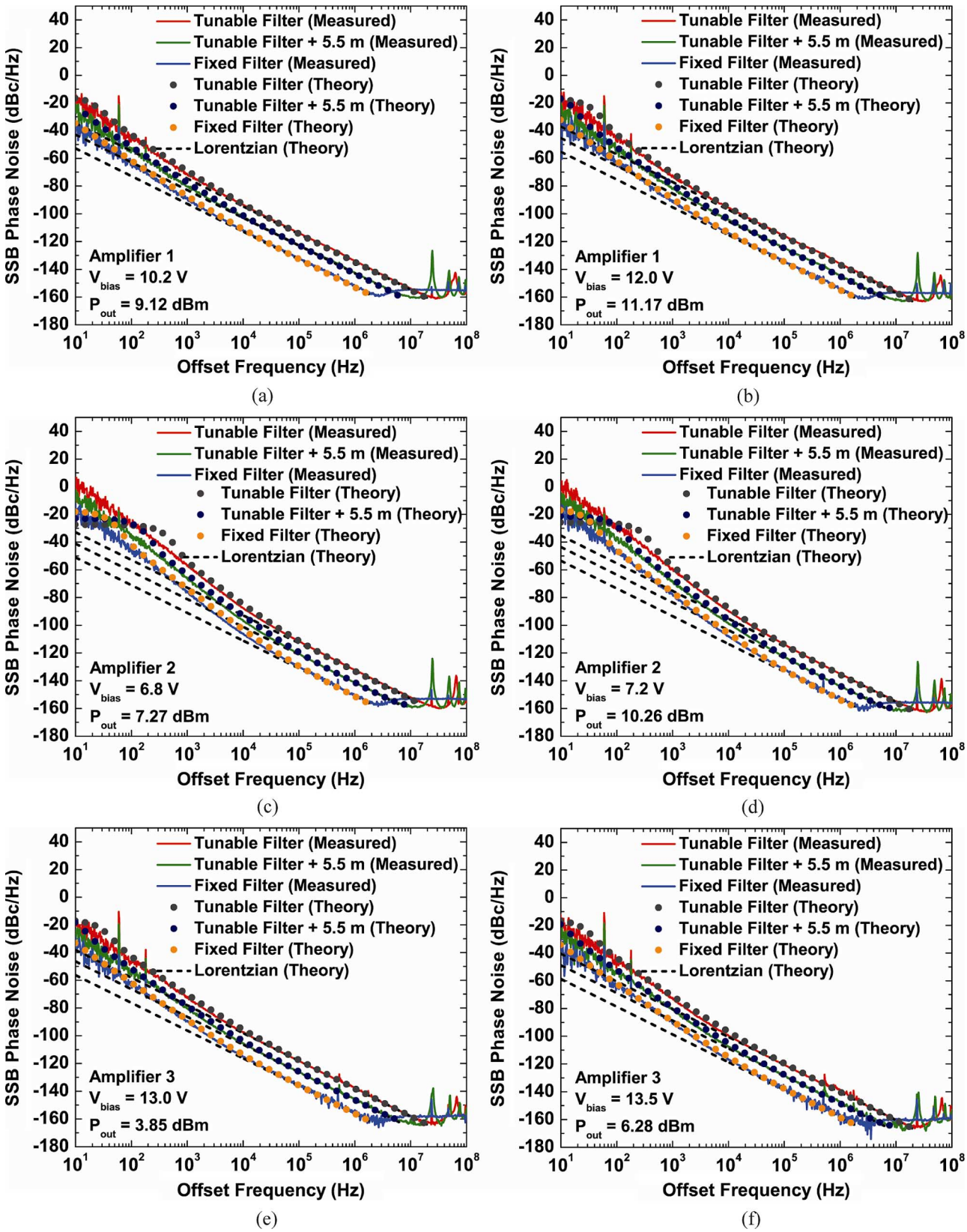

Fig. 3. Measured (solid lines) and theoretical (solid circles) RF oscillator phase-noise for three different types of amplifiers. (a) Phase noise for Amplifier 1 at 9.12 dBm RF power. (b) Phase noise for Amplifier 1 at 11.17 dBm RF power. (c) Phase noise for Amplifier 2 at 7.27 dBm RF power. (d) Phase noise for Amplifier 2 at 10.26 dBm RF power. (e) Phase noise for Amplifier 3 at 3.85 dBm RF power. (f) Phase noise for Amplifier 3 at 6.28 dBm RF power. The RF oscillator of Fig. 2 was tested with three filter configurations including 1) a tunable filter, 2) a tunable filter + 5.5 m delay, and 3) a fixed filter. The Lorentzian phase noise predictions (dashed line) are also shown.

It is apparent from Fig. 3 that all of the measured phase-noise spectra exhibit Lorentzian characteristics (20 dB/decade) at high offset frequencies but vary at a faster rate for frequencies closer to the carrier. This increase in phase-noise slope sig-

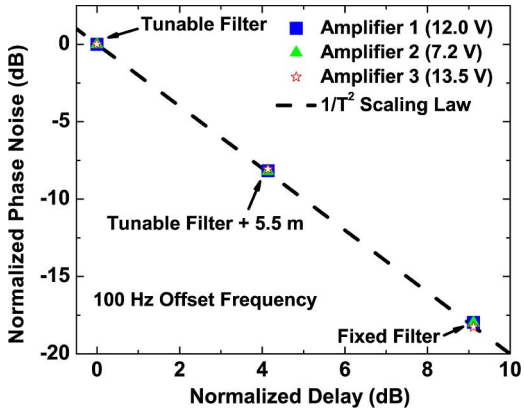

Fig. 4. Measured normalized phase noise at 100 Hz offset frequency as a function of the normalized delay for Amplifier 1 (12.0 V), Amplifier 2 (7.2 V), and Amplifier 3 (13.5 V). The phase noise is plotted for the tunable filter, tunable filter $+ 5.5\mathrm{m}$, and fixed filter configurations, normalized to the tunable filter case. The delay is similarly normalized to the delay of the tunable filter. The ideal $1/T^2$ dependency of phase noise on delay (dashed line) is also provided.

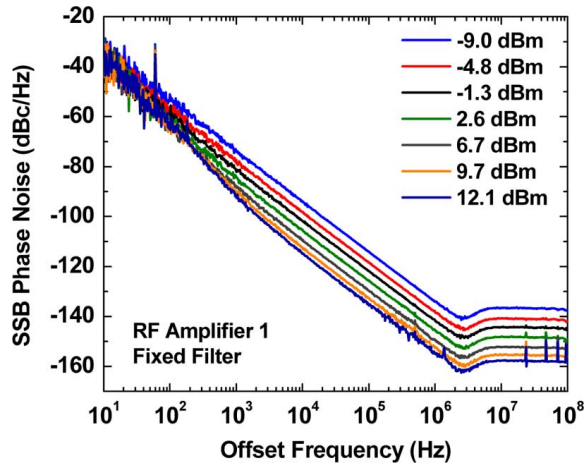

Fig. 5. Measured phase noise of a fixed filter oscillator as a function of RF output power. The system oscillates from gain supplied by Amplifier 1.

nifies the influence of flicker noise, as we shall see later. The inverse roundtrip delay associated with each filter configuration was estimated through the free-spectral-range corresponding to the sidemode spacing of the cavity. For the configurations comprising a tunable filter and a tunable $\mathrm{filter}{+}5.5\ \mathrm{m}$ delay, these inverse roundtrip times are 62.8 MHz and 24.2 MHz, respectively and remain approximately invariant across all three amplifiers. In the case of the fixed filter, the sidemodes cannot be observed as the RF filter is sufficiently narrow ($HW = 2.9$ MHz) to prevent power from accumulating at the sidemode frequencies. For these cases, the sidemode spacing can instead be estimated using the techniques described in Section II or by simply detuning the phase shifter until the sidemode appears relative to the oscillating mode. With these methods, the sidemode frequency was found to be approximately 7.7 MHz for all three oscillators that employ the fixed filter.

2) Phase-Noise Scaling With Delay: From the sidemode frequency, or equivalently the inverse roundtrip time, one can verify the scaling dependence of oscillator phase noise on T. The phase-noise scaling was previously found to be $1/T^2$ for white noise in [1], and this same dependence can also be observed in the measurements of Fig. 3. Taking as an example the Lorentzian contribution to Fig. 3(a), the measured phase-noise values at 1 MHz offset are $-134.1\ \mathrm{dBc/Hz}$ for the tunable filter, $-142.5\ \mathrm{dBc/Hz}$ for the tunable $\mathrm{filter} + 5.5\ \mathrm{m}$, and $-152.4\ \mathrm{dBc/Hz}$ for the fixed filter. Note that $1/T^2$ corresponds to a difference of 8.3 dB between the configurations of the tunable filter and tunable $\mathrm{filter} + 5.5\ \mathrm{m}$ and corresponds to a difference of 10 dB between the tunable $\mathrm{filter} + 5.5\ \mathrm{m}$ and the fixed filter.

These scaling relations also apply to the portions of the phase-noise spectrum due to flicker noise, as can be seen in all the measurements of Fig. 3. The corresponding results are consolidated in Fig. 4 for an offset frequency of 100 Hz from the carrier. In Fig. 4, the normalized phase noise is plotted as a function of the normalized delay for Amplifier 1 (12.0 V), Amplifier 2 (7.2 V), and Amplifier 3 (13.5 V). The delay is controlled by the configuration of the oscillator (tunable filter, tunable $\mathrm{filter} + 5.5\ \mathrm{m}$ delay, or fixed filter). Both the plotted phase noise and delay are normalized to their respective values for the tunable filter case. Ideally, one expects a 2 dB decrease in phase noise for every 1 dB increase in delay corresponding to a $1/T^2$ scaling dependence. We see that the measured results agree well with these predictions. This $1/T^2$ dependence also agrees with the form of (10)–(12) presented in Section II.

3) Phase-Noise Scaling With Power: An inverse relation also exists between phase noise and the corresponding signal power of the oscillator. This relationship can in principle be deciphered from Fig. 3 but is most easily seen in the measurements of Fig. 5. Fig. 5 shows the phase noise of a fixed filter oscillator as a function of the measured RF output power. The system uses the ring-cavity configuration of Fig. 2 and oscillates from gain supplied by Amplifier 1. The output power was varied through the bias voltage supplied to the amplifier. Note that the measured values of RF power represent directly the powers at the output of the amplifier. Similar to the fixed filter cases of Figs. 3(a) and 3(b), the sidemodes of Fig. 5 also cannot be observed in the phase-noise spectrum. In its place is the broadband white-noise added by the amplifier in a single roundtrip of the cavity. The filter prevents power from accumulating at frequencies beyond its passband. It is clear from Fig. 5 that the added white-noise floor decreases in direct proportion to the output power. In actuality, the added white noise remains approximately constant, and it is the normalization relative to carrier power that causes the noise floor to decrease with RF power. The observed clamping of the added white noise above threshold is analogous to the clamping of spontaneous emission in a laser [1], [3]. A similar dependence on carrier power can also be seen in the Lorentzian contribution to the spectrum at higher offset frequencies. The Lorentzian phase-noise is inversely related to signal power, as was both theoretically and experimentally shown in [1].

The properties of the Lorentzian phase noise are noticeably different from the noise characteristics at lower offset frequencies. At these offsets, upconverted flicker noise dominates over white noise, and the shape of the phase-noise spectrum changes to reflect this behavior. It is interesting to note that the phase

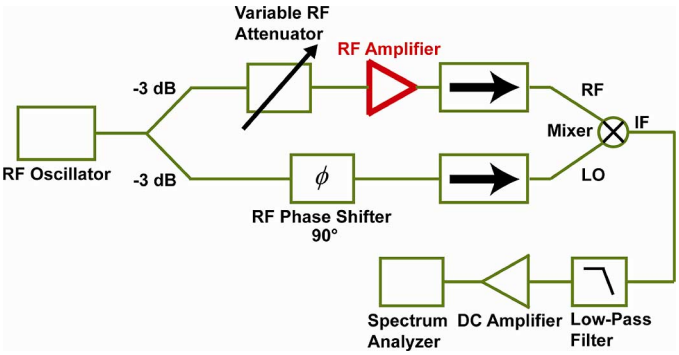

Fig. 6. Diagram of the system used to measure the residual phase-noise added by an RF amplifier.

noise at lower offsets appears somewhat constant and no longer depends inversely on carrier power (see Fig. 5). These results support our interpretation of flicker noise as a perturbation to the amplifier gain. A fluctuation in the gain propagates into all the modes of the oscillator supported by the gain. However, as this process is multiplicative (13), the upconverted noise that appears around a particular mode becomes approximately proportional to the strength of the mode. The end result is that the ratio of noise-to-signal remains relatively constant since the noise follows any increase or decrease in carrier power. Combining the properties of white and flicker noise then, we expect that their crossover point can be controlled through the RF power. This behavior is apparent in Fig. 5 and can also be observed directly in noise measurements of the amplifier itself [18].

4) Amplifier Noise Measurements: Next, we compare our theoretical predictions of oscillator phase-noise to the measurements of Fig. 3. For this comparison, (14) requires the phase-noise spectral density added in a single cavity roundtrip to be specified relative to the oscillation power $(N^{im}_{psd,tot}(\omega)/P_0)$. This quantity can be determined through a residual noise measurement of the amplifier phase noise (Fig. 6). In this measurement, a 2.5 GHz RF oscillator signal is equally split along two paths. The RF path probes the RF amplifier under test with an amount of power controllable by the variable RF attenuator. The LO path passes through an RF phase shifter maintaining quadrature between both arms. These two paths are combined in a double balanced mixer thereby generating a down-converted IF signal that is subsequently low-pass filtered to remove mixing harmonics. The resulting signal is then amplified (40 dB) and detected on an Agilent E4440A spectrum analyzer. The common-mode phase noise of the RF oscillator is rejected by the mixing process if the LO and RF paths are balanced in length. Similarly, the amplitude noise (of both the oscillator and the amplifier) is also suppressed by the saturated amplifier/mixer. The system of Fig. 6 then in principle measures only the added phase noise of the amplifier at its bias point of operation. In practice, the effects of amplitude noise and oscillator phase-noise are not completely suppressed and can both cause distortion to the results.

Fig. 7 shows the measured residual phase-noise for Amplifiers 1, 2, and 3 under the operating conditions (bias voltage and input RF power) used in Fig. 3. These measurements are calibrated by determining the system transfer function due to broadband noise injection. The resulting phase noise is normalized to the signal power for each of the cases in Fig. 7. It is clear that the phase noise measured all exhibit a similar general form. The low-frequency noise shows characteristics of $1/f^{\alpha}$, while the high-frequency noise flattens into a broadband floor of white noise. The spurs at harmonics of 60 Hz are due to the power line, while the feature near 5.5 kHz is due to noise present in the measurement system (ground loops, etc). In addition to these measured results, Fig. 7 also provides the asymptotic fits to the low—and high-frequency noise spectra. For the case of Amplifier 2, we use a slope of -10 dB/decade even though the actual noise shape varies at a slightly faster rate. This choice of flicker slope introduces a small error but allows for simpler noise calculations using (20) as we will see later. A summary of our results is provided in Table I.

As expected, the additive white phase-noise of each amplifier decreases in direct proportion to its corresponding carrier power. This is a consequence of the normalization such that the noise power appears lower relative to the signal. Since the operating conditions were made constant between the oscillator measurements of Fig. 3 and the amplifier measurements of Fig. 7, the white phase-noise levels between the two are directly comparable. Note that the values of the oscillator white phase-noise must be obtained from the fixed filter cases since the sidemodes are not completely extinguished using the tunable filter. The properties of flicker noise are harder to predict since the noise upconversion process depends on the characteristics of the amplifier (13). However in general, the ratio of noise to signal remains relatively constant over most of the frequency range since the upconversion process is multiplicative. For example, Table I shows that the flicker noise of Amplifier 1 extrapolated to 1 Hz offset is -130.1 dBc/Hz for $P_{out} = 2.42$ dBm and is -127.3 dBm for $P_{out} = 4.47$ dBm. Although this value has increased by 2.8 dB over a ~ 2 dB difference in power, the slope has also increased from -6.8 dB/decade to -8.4 dB/decade. The net result is that the noise at many of the intermediate frequencies does not change significantly in strength. It is interesting to note that Amplifier 2 exhibits the largest flicker noise (by ~ 20 dB), whereas the flicker noise of Amplifier 1 and 3 are similar. These properties can also be seen in the phase noise of the oscillators (Fig. 3) associated with Amplifiers 1, 2, and 3.

5) Comparisons of Theory to Measurement: We now use the measured noise properties of Amplifiers 1, 2, and 3 to predict the phase noise of their corresponding oscillators in Fig. 3. Most of this analysis follows from our discussions of (14)–(20). We will however mention a few of the important points in these calculations. First, the analysis of $1/f^{\alpha}$ noise for non-integer α follows similarly from (14)–(16). When $0 \leq \alpha < 1$, the integral from zero to infinity converges, and the effects of finite measurement time can usually be ignored to good approximation. Second, the flicker noise coefficient used in (14) is expressed in units of angular frequency. For $1/f^{\alpha}$ noise, the conversion from linear frequency to angular frequency results in a factor of $(2\pi)^{\alpha}$. And third, as discussed earlier, (20) for $1/f$ noise is only applicable when the autocorrelation of (16) vanishes in the large τ limit. In order to apply (20) to Amplifier 2 then, we would need to justify that this condition

TABLE I
SUMMARY OF RF AMPLIFIER RESIDUAL PHASE-NOISE MEASUREMENTS CORRESPONDING TO AMPLIFIERS 1, 2, AND 3

	P_{out}	V_{bias}	$1/f^{\alpha}$ at 1 Hz	White Noise	$1/f^{\alpha}$ Slope
Amplifier 1	9.12 dBm	10.2 V	-130.1 dBc/Hz	-154.4 dBc/Hz	-6.8 dB/decade
	11.17 dBm	12.0 V	-127.3 dBc/Hz	-156.3 dBc/Hz	-8.4 dB/decade
Amplifier 2	7.27 dBm	6.8 V	-105.5 dBc/Hz	-153.3 dBc/Hz	-10 dB/decade
	10.26 dBm	7.2 V	-108.3 dBc/Hz	-156.4 dBc/Hz	-10 dB/decade
Amplifier 3	3.85 dBm	13.0 V	-128.3 dBc/Hz	-158.1 dBc/Hz	-7.6 dB/decade
	6.28 dBm	13.5 V	-129.0 dBc/Hz	-161.0 dBc/Hz	-7.6 dB/decade

is satisfied. Let us do so by first revisiting the more general (19) and specifically evaluate the coefficient $C = N_1^{im}/\pi P_0 T^2$ Using $1/T = 7.7$ MHz and $N_1^{im}/P_0 = (2.82 \times 10^{-11}) \times 2\pi$ (Table I: Amplifier 2 at 6.8 V), we find C to be $\sim 3340\ 1/\mathrm{s}^2$. Furthermore, for τ ranging from 0 to 12.9 s corresponding to the SSA measurement time, we find that $\omega_c = 2\pi/12.9$ rad/s. With these values, it is clear that (19) evaluates to be much greater than unity (and thus (16) becomes negligible) in the limit of large τ. The use of (20) can be similarly justified for the remaining operating points of $1/T$ and N_1^{im}/P_0 corresponding to Amplifier 2. Note that $\tau = 12.9$ s corresponds to a lower frequency limit of 1 Hz offset for measurements in the SSA. This value coincides with our measurements in Fig. 3 even though the displayed frequency range has been limited to 10 Hz offset for ease of comparison to Fig. 7.

Fig. 3 shows both the calculated and measured phase noise for oscillators employing the three different RF amplifiers discussed previously. In the theoretical curves of Fig. 3, we have also included the Lorentzian prediction of phase noise (dashed line) due solely to white noise. These contributions were calculated using the theory of [1], or equivalently, by combining (18) with (16), normalizing by P_0, and taking the Fourier transform. The parameters used for this calculation consist of the measured noise-to-signal ratios of Table I and the estimated values of roundtrip delay discussed previously. By comparing the Lorentzian curves to measurement, we see that the high frequency behavior of oscillator phase-noise is accurately captured, whereas large differences are observed at low frequency offsets. These inadequacies at low frequencies are resolved by accounting for the effects of flicker noise using the full theory of oscillator phase-noise (solid circles). As is apparent in Fig. 3, the agreement of the full theory with measurement is excellent (< 1 dB for white noise, < 3 dB for flicker noise) over most of the frequency range. However, deviations are still present below 100 Hz for Amplifiers 1 and 3 and below 1 kHz for Amplifier 2. These deviations arise from discrepancies in the definition of phase noise (described next) rather than from any source of errors in our prediction.

Currently, there are two definitions of phase noise used throughout literature: (1)$S_E(\omega)$- the spectral density of the field and (2)$S_\phi(\omega)$- the spectral density of the phase. $S_E(\omega)$ is the quantity calculated from (14)–(16) as we have taken an autocorrelation in the oscillator field. On the other hand, measurements of phase noise effectively find $S_\phi(\omega)$ instead. This can be shown by calculating the mixer output voltage (IF) corresponding to the measurement and subsequently determining the spectrum of the result (see Appendix). $S_E(\omega)$ and $S_\phi(\omega)$ are approximately equal at higher offset frequencies but deviate from each other at frequencies close to the carrier. In particular, $S_E(\omega)$ clips at low frequencies attesting that the oscillator spectrum is bounded. This behavior is clearly visible in Figs. 3(c) and 3(d) but can also be seen in the other measurements of Fig. 3. Note that $S_\phi(\omega)$ is unbounded at low frequencies reaching measured values of 25 dBc/Hz at 1 Hz offset (not shown) for Amplifier 2. As expected, these values cannot correspond to physical measures of the oscillator field spectrum as they would imply the noise power integrated over 1 Hz would be larger than the total power available to the carrier. Combined with the fact that real systems typically work with periodic functions of phase rather than any direct phase variable, we regard $S_E(\omega)$ to be more fundamental than $S_\phi(\omega)$.

B. Comparisons to Measurement: Optoelectronic Oscillator

In this section, we apply (14)–(16) to a hybrid optoelectronic oscillator (OEO) in order to demonstrate the generality of the theory. The OEO (Fig. 8) comprises both optical and electrical cavity elements, and net gain is achieved via a combination of microwave-photonic (MWP) gain [21] and RF amplification. The OEO is driven by a high-power low-noise slab-coupled optical waveguide external cavity laser (SCOWECL) [22], [23] ($P = 150$ mW at 2-A bias) whose power is controlled by a variable optical attenuator (VOA). The other elements of the optical cavity consist of a Mach-Zehnder (MZ) modulator ($BW = 15$ GHz, $V_\pi = 3.1$ V at 3 GHz), an optical isolator, and a commercial photodiode ($\Re = 0.8$ A/W, $BW = 12$ GHz). Typically, an OEO would also employ a long optical fiber delay for the goal of obtaining low phase-noise. We have excluded this element within our cavity as the phase noise becomes too low to measure compared to the SSA noise floor. In the electrical path, the photodiode output is amplified by a low flicker-noise AML26PNB2001 $2-6$ GHz RF amplifier ($G = 23.4$ dB, small-signal $NF = 5.7$ dB) and coupled out through a -10 dB RF tap. The remainder of the power (90%) is recirculated within the cavity first to an RF phase shifter and subsequently to a 3 GHz RF filter ($HW = 1.2$ MHz). The optoelectronic loop is closed by feeding the RF signal back as input drive to the MZ modulator. Oscillation begins from the amplification of noise incident on the modulator RF input port. Similar to the RF oscillator cases discussed in the previous section, the noise is coupled out before passing through the filter. This allows the white noise of a single roundtrip to be directly measured from the oscillator output [1].

The MWP gain in an OEO results from a two-step process where the CW (pump) laser source is first modulated by an RF

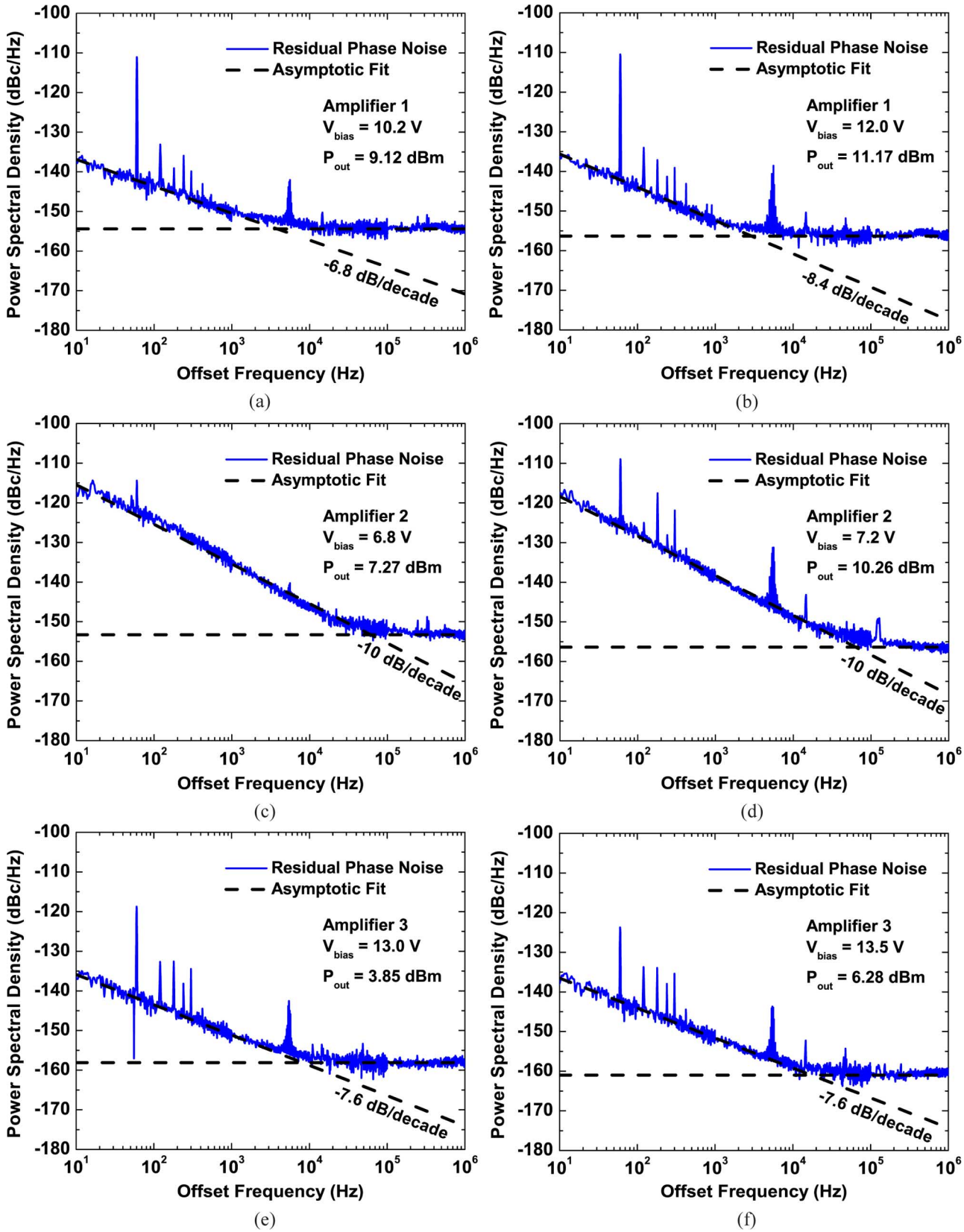

Fig. 7. Measured phase noise (solid line) with asymptotic fits (dashed line) for three different types of RF amplifiers. (a) Amplifier 1 phase noise with 9.12 dBm output RF power. (b) Amplifier 1 phase noise with 11.17 dBm output RF power. (c) Amplifier 2 phase noise with 7.27 dBm output RF power. (d) Amplifier 2 phase noise with 10.26 dBm output RF power. (e) Amplifier 3 phase noise with 3.85 dBm output RF power. (f) Amplifier 3 phase noise with 6.28 dBm output RF power. The phase-noise slope is also indicated for each case.

input generating sidebands around the optical carrier. The RF information is later recovered after photodetection from the heterodyning of the sidebands with the carrier. For a given frequency, net gain is achieved if the signal amplitude increases

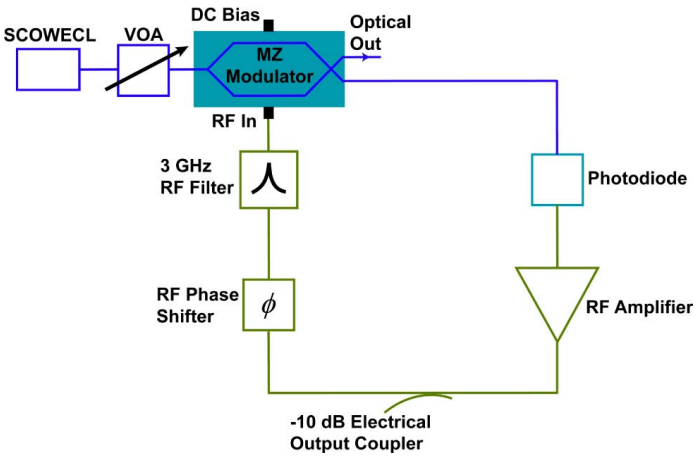

Fig. 8. Configuration of an optoelectronic oscillator (OEO) operating at 3.0 GHz. Microwave-photonic (MWP) gain is achieved by the highpower, low-noise slab-coupled optical waveguide external cavity laser (SCOWECL), Mach-Zehnder modulator (MZ Modulator) and photodiode.

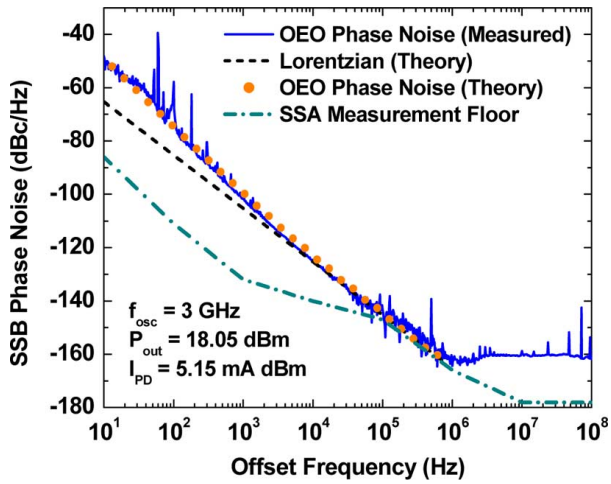

Fig. 9. Measured (solid line) and theoretical (solid circles) phase noise of an OEO corresponding to the configuration of Fig. 8.

from RF in to RF out. This process can be described through [9], [12]

$$V_{out} = V_{supply} \frac{J_1\left(\frac{\pi V_{in}}{V_\pi}\right)}{V_{in}} V_{in} \tag{21}$$

where $V_{out}(V_{in})$ is the amplitude of the sinusoidal output (input) voltage and V_π is the MZ modulator half-wave switching voltage. $V_{supply} = P_O \sin(\Gamma_0)\, \alpha \Re R$ consists of a product between the optical power supplied by the laser (P_O), the sine of the MZ modulator bias angle $(\sin \Gamma_0)$, the optical attenuation accumulated from signal propagation to the photodiode (α), the photodiode responsivity $(\Re)$, and the photodiode load resistance (R).

Equation (21) expresses that the MWP voltage gain from V_{in} to V_{out} is dependent on the supplied voltage (V_{supply}) and a saturation parameter $(J_1(\pi V_{in}/V_\pi)/V_{in})$. If $V_{in} << V_\pi$, this saturation parameter evaluates to a constant $\pi/2V_\pi$. However, for larger values of V_{in}, the gain quickly compresses below its small signal value. It is clear that (21) exhibits a similar functional form compared to the gain model introduced in (13) with $\Delta G(t)$ representing noise on the supply voltage. A low-frequency relative intensity noise (RIN) fluctuation of the SCOWECL source becomes directly upconverted into a fluctuation on the carrier. This process occurs in conjunction with the additive white noise that directly perturbs the OEO.

Here, we are interested in comparing measurements of the OEO phase-noise to predictions obtained from (14)–(16). Fig. 9 shows the measured 3 GHz OEO phase-noise along with the noise floor of the SSA measurement. The SCOWECL was operated at 2 A bias, while the intracavity attenuation was adjusted to maintain 5.15 mA photocurrent. The OEO phase-noise shows characteristics corresponding to a Lorentzian (20 dB/decade) at high frequencies but falls off at a faster rate at low frequencies. These phase-noise properties are indicative of a transition from white noise to flicker noise in the spectrum of injected noise. The SSA noise floor also suggests that the measured phase noise between 100 kHz and 1 MHz is slightly high due to influence from the noise of the measurement system. As was found for the fixed filter cases of the RF oscillator, the cavity sidemodes are again rejected here by the narrow passband of the 3 GHz filter. Separate measurements of the sidemode frequency spacing, however, determine its value to be near 3.6 MHz.

In order to calculate the OEO phase-noise, we require knowledge of the injected noise in a single roundtrip of the cavity. The added noise is the combined total from contributions of the MWP link and also from that of the RF amplifier. We may treat their combination as an equivalent amplifier providing gain from RF in to RF out. The phase noise of the combined amplifier can be probed using the system of Fig. 10(a) in an analogous manner to a conventional amplifier (Fig. 6). For this measurement, the individual components of the amplifier are driven under their respective OEO operating conditions. This yields 14.3 dBm RF input into the MZ modulator and 18.1 dBm RF output after the RF amplifier. The measured phase noise of the combined amplifier is shown in Fig. 10(b). We have also provided the noise floor of the measurement, which can be seen to slightly increase the noise at low offset frequencies. The phase noise extrapolated to 1 Hz offset is found to be $-138.4\ \mathrm{dBc/Hz}$ with a slope of $-5.8\ \mathrm{dB/decade}$. This noise level is lower than that of conventional RF amplifiers (Fig. 7) due to the use of low-noise components in the MWP link and also to the use of a low flicker-noise RF amplifier. The white phase-noise floor of the combined amplifier is $-161\ \mathrm{dBc/Hz}$ and matches the level of white noise found in Fig. 9. Note that both the noise feature near 5.5 kHz and the spurs at 60 Hz harmonics can again be observed in the measurements of Fig. 10(b).

Using the measured amplifier noise characteristics, we can now predict the phase noise of the OEO. These calculations closely mirror that of the RF oscillator in Figs. 3 and 7. Thus, we will only present their results which are illustrated in Fig. 9. When only white noise is taken into account, the spectrum is a Lorentzian (dashed line) and agrees well with the measured OEO phase-noise at higher offset frequencies. At low frequencies where the influence of flicker noise begins to dominate, the agreement quickly degrades. On the other hand, the full theory (solid circles) accurately captures the effects of both white and flicker noise and therefore shows excellent

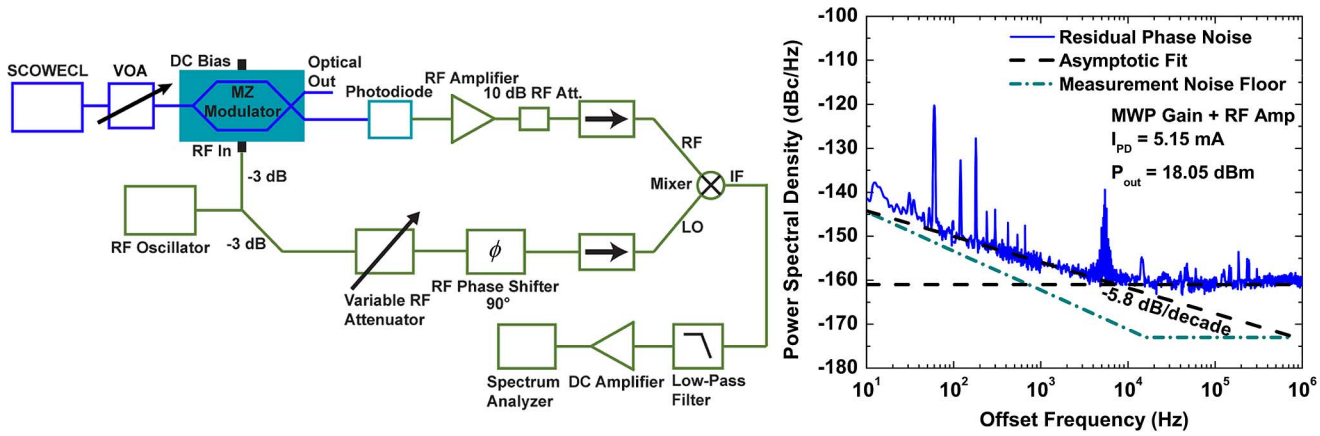

(a) (b)

Fig. 10. (a) Circuit schematic and (b) measured results for single-pass OEO residual phase-noise. The measurement system is similar to that of Fig. 6 but measures the phase noise of the combined amplifier (MWP link + RF amplifier). In addition to the OEO residual noise (solid line), the asymptotic fit (dashed line) and measurement noise floor (dash-dot line) are also provided.

agreement to measurement. The OEO phase-noise is lower than that corresponding to the RF oscillators of Fig. 3 even with no intentionally added optical delay. With a factor of 10–100 increase in delay, the phase noise can be improved by 20–40 dB. Using optical fiber, this can all be achieved suffering only small penalties in loss.

IV. Conclusion

We have presented a general theory of oscillator phase-noise when the perturbation is driven by sources of white and flicker noise. The upconversion of low-frequency noise is treated from the perspective of a gain perturbation which then couples into the modes of the oscillator. We apply the theory to several cases of RF oscillators varying between their RF amplifiers used and the configuration of their RF filter. The phase noise of each oscillator was also tested at two separate operating points in oscillation power. With knowledge of the oscillation power, roundtrip delay, and corresponding injected noise spectrum, the oscillator phase-noise was predicted to excellent accuracy. The theory was also applied to a hybrid optoelectronic oscillator as a demonstration to its generality. Excellent agreement was again found in this case. Although only electromagnetic oscillators were tested in this work, the theory can be extended to oscillators of other varieties.

Appendix

Derivation of the Mixer (IF) Voltage Output: We begin by considering the voltage of an oscillator defined through

$$V_{RF} = V_0 \sin\left(\omega_0 t + \theta_0(t)\right) \tag{A.1}$$

incident on the RF arm of an ideal mixer. Here, ω_0 defines the frequency of oscillation. In (A.1), we ignore the effects of amplitude noise on the oscillation amplitude V_0 and use $\theta_0(t)$ to account for fluctuations of the oscillator's phase. Imagine now that one wishes to measure the phase noise using a suitably low noise reference oscillator. The reference is sent into the LO arm of the mixer and is phase locked to the original oscillator waveform so that both oscillators share the same operating frequency. The mixer is also biased at quadrature enforcing the LO voltage at ω_0 to follow a cosine response pattern. The operation of the mixer then generates an IF voltage that consists of the product between the individual RF and LO signals

$$\begin{aligned} V_{IF} &= \alpha_m V_0 \sin\left(\omega_0 t + \theta_0(t)\right) \cos\left(\omega_0 t + \theta_{ref}(t)\right) \\ &= \frac{\alpha_m V_0}{2} \sin\left(\theta_0(t) - \theta_{ref}(t)\right) \\ &\quad + \frac{\alpha_m V_0}{2} \sin\left(2\omega_0 t + \theta_0(t) + \theta_{ref}(t)\right). \end{aligned} \tag{A.2}$$

In (A.2), $\theta_{ref}(t)$ represents the phase fluctuations of the reference oscillator, which closely tracks $\theta_0(t)$ by action of the phase-locked loop. We have also introduced α_m to account for losses during the mixing process. The IF signal is subsequently low-pass filtered

$$V_{IF}^{LP} = \frac{\alpha_m V_0}{2} \sin\left(\theta_0(t) - \theta_{ref}(t)\right) \tag{A.3}$$

retaining only the contributions near DC. Detection of V_{IF}^{LP} using a spectrum analyzer yields the desired phase-noise spectrum of the oscillator.

Upon comparing (A.3) to (A.1), we see that V_{IF}^{LP} is a scaled, frequency-shifted, and *biased* version of the original oscillator voltage V_{RF}. If $\theta_{ref}(t)$ is independent from $\theta_0(t)$ and also much lower in magnitude, this measurement would yield approximately the phase-noise spectrum of the original oscillator. In other words, one can always beat two oscillators together and measure the noise of the lower-performing system. If however $\theta_{ref}(t)$ is correlated with $\theta_0(t)$ as would be the case using a phase-locked loop, then the measured spectrum becomes distorted by the degree of correlation. For perfect correlation $(\theta_{ref}(t) = \theta_0(t))$, V_{IF}^{LP} becomes 0. This means that the measured phase noise vanishes when one mixes an oscillator with its twin.

Under normal operating conditions, $\theta_{ref}(t)$ and $\theta_0(t)$ are only partially correlated and only within the phase-locked loop bandwidth. In these cases, $\theta_0(t) - \theta_{ref}(t)$ is small (but non-zero), and the measured phase-noise spectrum becomes suppressed for offset frequencies within the loop

bandwidth. The significance is that measuring the spectrum of $V_{IF}^{(LP)}$ is effectively equivalent to measuring the spectrum of $\theta_0(t) - \theta_{ref}(t)$ by virtue of the small-angle approximation. When the phase tracking of the reference oscillator is later accounted for in post-analysis by correcting for the distortion at low offset frequencies, the spectral density corresponding to $\theta_0(t)$ is recovered. Our analysis therefore shows that it is the spectral density of phase that is determined in an oscillator phase-noise measurement. Note that this is only true if both the small-angle approximation is applicable ($\theta_{ref}(t)$ tracks $\theta_0(t)$) *and* post-analysis correction is used on the measured spectrum. These conditions apply to most measurements of oscillator phase noise but do not apply when the spectrum is directly detected by a spectrum analyzer. In this case, no mechanism of phase tracking exists, and it is the spectral density of the field that is found.

REFERENCES

[1] W. Loh, S. Yegnanarayanan, R. J. Ram, and P. W. Juodawlkis, "Unified theory of oscillator phase noise I: white noise," *IEEE Trans. Microw. Theory Tech.*, vol. 61, no. 6, pp. 2371–2381, Jun. 2013.

[2] C. H. Henry, "Theory of the linewidth of semiconductor lasers," *IEEE J. Quantum Electron.*, vol. 18, no. 2, pp. 259–264, Feb. 1982.

[3] L. A. Coldren and S. W. Corzine, *Diode Lasers and Photonic Integrated Circuits*. New York, NY, USA: Wiley, 1995, pp. 140–241.

[4] M. J. O'Mahony, "Semiconductor laser linewidth broadening due to 1/f carrier noise," *Electron. Lett.*, vol. 19, pp. 1000–1001, Nov. 1983.

[5] L. B. Mercer, "1/f frequency noise effects on self-heterodyne linewidth measurements," *J. Lightw. Technol.*, vol. 9, no. 4, pp. 485–493, Apr. 1991.

[6] A. Demir, "Phase noise and timing jitter in oscillators with colored-noise sources," *IEEE Trans. Circuits Syst. I, Fundam. Theory Applicat.*, vol. 49, no. 12, pp. 1782–1791, Dec. 2002.

[7] A. Demir, "Computing timing jitter from phase noise spectra for oscillators and phase-locked loops with white and 1/f noise," *IEEE Trans. Circuits Syst. I, Reg. Papers*, vol. 53, no. 9, pp. 1869–1884, Sep. 2006.

[8] F. X. Kaertner, "Analysis of white and $f^{-\alpha}$ noise in oscillators," *Int. J. Circuit Theory Appl.*, vol. 18, no. 5, pp. 485–519, Sep. 1990.

[9] X. S. Yao and L. Maleki, "Optoelectronic microwave oscillator," *J. Opt. Soc. Amer. B*, vol. 13, no. 8, pp. 1725–1735, Aug. 1996.

[10] L. Maleki, "Sources: the optoelectronic oscillator," *Nature Photon.*, vol. 5, pp. 728–730, Dec. 2011.

[11] W. Loh *et al.*, "Amplifier-free slab-coupled optical waveguide optoelectronic oscillator systems," *Opt. Exp.*, vol. 20, no. 17, pp. 19589–19598, Aug. 2012.

[12] W. Loh, S. Yegnanarayanan, R. J. Ram, and P. W. Juodawlkis, "Super-homogeneous saturation of microwave-photonic gain in optoelectronic oscillator systems," *IEEE Photon. J.*, vol. 4, no. 5, pp. 1256–1266, Oct. 2012.

[13] P. Langevin, "Sur la théorie de movement brownien," *C. R. Acad. Sci. Paris*, vol. 146, pp. 530–533, 1908.

[14] F. D. Martini and G. R. Jacobovitz, "Anomalous spontaneous-stimulated-decay phase transition and zero-threshold laser action in a microscopic cavity," *Phys. Rev. Lett.*, vol. 60, no. 17, pp. 1711–1714, Apr. 1988.

[15] H. Yokoyama *et al.*, "Controlling spontaneous emission and threshold-less laser oscillation with optical microcavities," *Opt. Quantum Electron.*, vol. 24, no. 2, pp. S245–S272, 1992.

[16] H. Nyquist, "Thermal agitation of electric charge in conductors," *Phys. Rev.*, vol. 32, no. 1, pp. 110–113, Jul. 1928.

[17] B. M. Oliver, "Thermal and quantum noise," *Proc. IEEE*, vol. 53, no. 5, pp. 436–454, Jul. 1965.

[18] R. Boudot and E. Rubiola, "Phase noise in RF and microwave amplifiers," *IEEE Trans. Ultrason. Ferroelec. Freq. Contr.*, vol. 59, no. 12, pp. 2613–2624, Dec. 2012.

[19] S. Kogan, *Electronic Noise and Fluctuations in Solids*. Cambridge, U.K.: Cambridge Univ. Press, 1996, pp. 203–286.

[20] D. S. Elliot, R. Roy, and S. J. Smith, "Extracavity laser band-shape and bandwidth modification," *Phys. Rev. A*, vol. 26, no. 1, pp. 12–18, Jul. 1982.

[21] C. H. Cox, III, *Analog Optical Links: Theory and Practice*. Cambridge, U.K.: Cambridge Univ. Press, 2004, ch. 3.

[22] W. Loh *et al.*, "Packaged, high-power, narrow-linewidth slab-coupled optical waveguide external cavity laser (SCOWECL)," *IEEE Photon. Technol. Lett.*, vol. 23, no. 14, pp. 974–976, Jul. 2011.

[23] P. W. Juodawlkis *et al.*, "High-power, low-noise 1.5 μm slab-coupled optical waveguide (SCOW) emitters: physics, devices, and applications," *IEEE J. Sel. Top. Quantum Electron.*, vol. 17, no. 6, pp. 1698–1714, Nov. 2011.

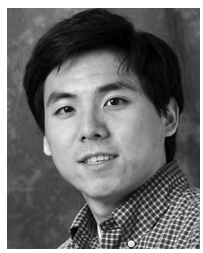

William Loh received the B.S. degree in electrical engineering from the University of Michigan, Ann Arbor, MI, USA, in 2007, and the M.S. degree in electrical engineering from the Massachusetts Institute of Technology (MIT), Cambridge, MA, USA, in 2009. He is currently pursuing the Ph.D. degree in electrical engineering as an active member of the Integrated Photonics Initative (IPI) collaboration between the MIT Lincoln Laboratory and the MIT campus.

His research interests include novel structures and schemes for semiconductor optical devices, microwave-photonic oscillators for synthesis of low-noise RF signals, physics of noise processes in oscillators and optoelectronic systems, and modeling of optical phenomena in photonic systems and devices.

Siva Yegnanarayanan (S'92–M'00) received the B.S. degree from Indian Institute of Technology (IIT), Madras, India, the M.S. degree from University of Maryland Baltimore County, MD, USA, and the Ph.D. degree from the University of California, Los Angeles, CA, USA, all in electrical engineering.

He was a Staff Scientist at Alcatel Corporate Research Center from 1999–2000. He joined Cognet Microsystems Inc. in 2000 and was at Intel Corporation from 2001–2004. Subsequently, he was a Staff Scientist in the Photonics Research Group at Georgia Institute of Technology from 2004–2010. He joined the Electro-Optical Materials and Devices Group, Lincoln Laboratory, Massachusetts Institute of Technology (MIT), Lexington, MA, USA, in 2010, where he is a member of the technical staff. His current research interests include microwave photonics, coherent photonic devices and sub-systems, high-power waveguide photodiodes, high-power semiconductor optical amplifiers and their application in mode-locked lasers, and narrow-linewidth external-cavity lasers.

Dr. Yegnanarayanan is a member of the Optical Society of America.

Rajeev J. Ram received the B.S. degree in applied physics from the California Institute of Technology, Pasadena, CA, USA, in 1991 and the Ph.D. degree in electrical engineering from the University of California, Santa Barbara, CA, USA, in 1997.

He is currently a professor at the Massachusetts Institute of Technology, Cambridge, MA, USA, where he is Associate Director of the Research Laboratory of Electronics and director of the Center for Integrated Photonics Systems. His research focuses on physical optics and electronics, including the development of novel components and systems for communications and sensing, novel semiconductor lasers for advanced fiber optic communications, and studies of fundamental interactions between electronic materials and light.

Paul W. Juodawlkis (S'86–M'86–SM'06) received the B.S. degree from Michigan Technological University, Houghton, MI, USA, the M.S. degree from Purdue University, West Lafayette, IN, USA, and the Ph.D. degree from the Georgia Institute of Technology, Atlanta, GA, USA, all in electrical engineering.

From 1988 to 1993, he was a Technical Staff Member at Lincoln Laboratory, Massachusetts Institute of Technology (MIT), Lexington, MA, USA, where he was a Hardware Systems Engineer on a multi-sensor airborne testbed program. He then joined the Ultrafast Optical Communications Laboratory (UFOCL), Georgia Institute of Technology. In 1999, he rejoined the Lincoln Laboratory, MIT, as a member of the Electro-Optic Materials and Devices Group. He is currently Assistant Group Leader of the Electro-Optic Materials and Devices Group at the Lincoln Laboratory, MIT, where he is leading research on semiconductor optoelectronic devices and microwave photonics. His research efforts have focused on the development of optical sampling techniques for photonic analog-to-digital converters (ADCs), quantum-well electrorefractive modulators, high-power waveguide photodiodes, and high-power semiconductor optical amplifiers (SOAs) and their application in mode-locked lasers and narrow-linewidth external-cavity lasers.

Dr. Juodawlkis was General Co-Chair of the 2012 Conference on Lasers and Electro-Optics (CLEO) and Program Co-Chair of the 2010 CLEO. He is currently a member of the IEEE Photonics Society Board of Governors (2011–2013). He has served as Chair of the IEEE Photonics Society Technical Committee on Microwave Photonics (2003–2006), Program Co-Chair of the 2003 Photonics Society Summer Topical Meeting on Photonic Time/Frequency Measurement and Control, and Program Committee Member of the Optical Fiber Communication (OFC) conference (2013) and the International Topical Meeting on Microwave Photonics (2004, 2008, 2013). He is also a member of the Optical Society (OSA) and the American Association for the Advancement of Science (AAAS).